Renewable Energy 59 (2013) 13–22

Contents lists available at SciVerse ScienceDirect

Renewable Energy

journal homepage: www.elsevier.com/locate/renene

Analysis of alternative adaptive geometrical configurations for the NREL-5 MW wind turbine blade

Lucas I. Lago [a], Fernando L. Ponta [a,*], Alejandro D. Otero [b,a]

[a] Department of Mechanical Engineering – Engineering Mechanics, Michigan Technological University, 1400 Townsend Dr, Houghton, MI 49931, United States
[b] CONICET & College of Engineering, University of Buenos Aires, Argentina

ARTICLE INFO

Article history:
Received 12 June 2012
Accepted 4 March 2013
Available online 11 April 2013

Keywords:
Wind turbine
Blade aeroelastic modeling
Blade adaptiveness
Generalized Timoshenko model
Innovative BEM theory implementation

ABSTRACT

The correct prediction of flexo-torsional deformation is of capital importance for the future development of advanced wind-turbine blade prototypes. Coupling between bending and twisting can be used to reduce extreme loads and improve fatigue performance. This is the principle of the adaptive blades, where the incremental loads are reduced when, as the blade bends, the flexo-torsional modes of the blade structure produce a change in twist, and so in the angle of attack, modifying the lift force acting on the blade sections. Bend-twist coupling could be achieved either by modifying the internal structure (structural adaptiveness), or by readapting the geometry of the blade (geometrical adaptiveness). These two techniques can be used independently or combined, complementing each other.

We have developed a novel computational tool for the aeroelastic analysis of wind-turbine blades, which allows a full representation of the flexo-torsional modes of deformation of the blade as a complex structural part and their effects on the aerodynamic loads. In this paper, we report some recent results we have obtained applying our code to the analysis of geometrical adaptive blades, taking full advantage of the coupled deformation modes that our aeroelastic code can represent. We analyze alternative blade configurations for the NREL-5 MW wind-turbine, optimizing the design to mitigate vibration and improve fatigue performance.

1. Introduction

Output power of the state-of-the-art wind turbines nowadays is in the range from 3.6 to 6 MW, with rotor diameters up to 127 m. Commercial models within this range are available from several manufacturers like GE, RE-Power, Enercon, Vestas and Siemens. This spontaneous tendency in the wind-turbine industry to increase the size of the state-of-the-art machine is driven by economies-of-scale factors that substantially reduce the cost of wind energy. The technological challenge in wind power nowadays is to develop a next generation of feasible upscaled turbines of cheaper construction that may further reduce generation costs. Now, industry insiders are talking about next-generation offshore turbine giants of 7.5–12 MW with rotor diameters close to 200 m [1]. If this generation of super-turbines is successfully developed, wind-energy costs would be reduced substantially. In favorable sites, it might be even feasible to produce hydrogen as a substitute fuel in competitive terms, helping to close the gap between the global fuel needs and the maximum amount of biofuel that may be produced sustainably.

But limitations in the current blade technology constitute a technological barrier that needs to be broken in order to continue the improvement in wind-energy cost. Blade manufacturing is mostly based on composite laminates, which is labor-intensive and requires highly-qualified manpower. It constitutes a bottleneck to turbine upscaling that reflects into the increasing share of the cost of the rotor, within the total cost of the turbine, as turbine size increases. Fig. 1 shows a compilation of data by NREL-DOE [2] on the proportional cost of each subsystem for different sizes of wind-turbines, where the systematic increase of the rotor cost share is clearly reflected. This increment is mainly commanded by the differences in scaling between different characteristics of the turbines. For example, the power of the turbine grows as the square of rotor size, but the weight of the components and, in particular, the blades would scale with the cube of the rotor size if geometric similarity is to be maintained. This situation is referred as the *square–cube law* [see Ref. [3], for example]. However, the WindPACT blade scaling study [4] showed that blade mass has been scaling at roughly an exponent of 2.3 instead of the expected 3. This is the reason why the cost share of blades has increased significantly but not as much as the *square–cube law* would predict.

* Corresponding author. Tel.: +1 9064873563.
E-mail address: flponta@mtu.edu (F.L. Ponta).

0960-1481/$ – see front matter © 2013 Elsevier Ltd. All rights reserved.
http://dx.doi.org/10.1016/j.renene.2013.03.007

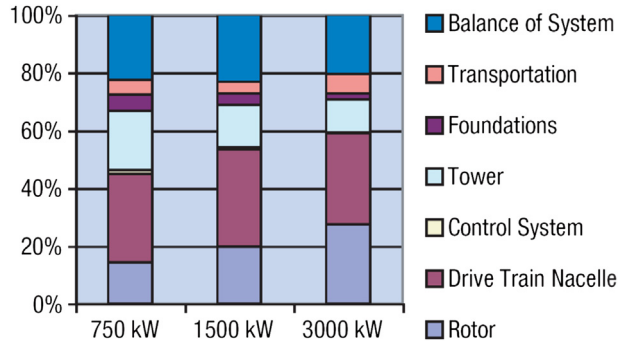

Fig. 1. Evolution of the proportional cost for the different wind-turbine subsystems, as size increases (data compilation from Ref. [2]).

A key factor for a breakthrough in wind-turbine technology is to reduce the uncertainties related to blade dynamics, by the improvement of the quality of numerical simulations of the fluid–structure interaction process, and by a better understanding of the underlying physics. The current state-of-the-art is to solve the aeroelastic equations in a fully non-linear coupled mode using Bernoulli or Timoshenko beam models (see Ref. [5], where a thorough coverage of the topic is presented). The goal is to provide the industry with a tool that helps them to introduce new technological solutions to improve the economics of blade design, manufacturing and transport logistics, without compromising reliability. A fundamental step in that direction is the implementation of structural models capable of capturing the complex features of innovative prototype blades, so they can be tested at realistic full-scale conditions with a reasonable computational cost. To this end, we developed a code based on a combination of two advanced numerical models implemented in a parallel HPC supercomputer platform: First, a model of the structural response of heterogenous composite blades [6], based on a variation of the dimensional reduction technique proposed by Hodges and Yu [7,8], which allows a full representation of the flexo-torsional modes of deformation. This technique has the capacity of reducing the geometrical complexity of the blade section into a stiffness matrix for an equivalent beam. The reduced 1-D strain energy is equivalent to the actual 3-D strain energy in an asymptotic sense, allowing accurate modeling of the blade structure as a 1-D finite-element problem. This substantially reduces the computational effort required to model the structural dynamics at each time step. Second, a novel aerodynamic model based on an advanced implementation of the BEM (Blade Element Momentum) Theory; where all velocities and forces are re-projected through orthogonal matrices into the instantaneous deformed configuration to fully include the effects of large displacements and rotation of the airfoil sections into the computation of aerodynamic forces. This allows the aerodynamic model to take into account the effects of the complex flexo-torsional deformation of the blade structure that can be captured by the more sophisticated structural model mentioned above.

The correct prediction of this flexo-torsional deformation is of capital importance for the future development of advanced blade prototypes. When the blade twists under load, the angle of attack changes, modifying the lift force, which constitutes the main component of aerodynamic load. As in an aircraft wing, this aeroelastic mechanism could be potentially dangerous if the blade structure is not properly designed. However, coupling between bending and twisting can be used to reduce extreme loads and improve fatigue performance. This is the principle of the *adaptive blades* (see Refs. [9,10], among others), where the incremental loads are reduced when, as the blade bends, the flexo-torsional modes of the blade structure produce a decrease in the blade twist, and so, the angle of attack. The level of load reduction could be controlled by two means: In the so-called *structural adaptiveness*, the level of bend-twist coupling depends on the blade cross-sectional geometry, the level of anisotropy in the structural material, and the material distribution [10]. In the so-called *geometrical adaptiveness*, the way to achieve bend-twist coupling is by readapting the geometry of the blade building it in a curved shape [11]. These two techniques can be used independently or combined, complementing each other.

Geometrical tailoring of the *flexo-torsional* or *bend-twist* coupling is a concept originally coming from aeronautics. Fine tuning of the relative positions between the structural torsional center of the blade section and its aerodynamic center (conventionally located at the quarter-chord length for typical airfoils) is one of the main principles of *swept wings* to avoid the so-called *structural divergence* and self-adapt angles of attack on the wing sections. This concept was originally developed in Germany in the 1930s [12,13] and deeply researched during the days of World War II. There are two possible configurations on swept wings, the first is known as backwards sweeping. This became almost universal for light planes, jet fighters, bombers, and commercial aircraft flying under the subsonic and transonic regimes. The main characteristic of this configuration is that the aerodynamic coefficient reference point is located behind the wing section's torsional center resulting in a natural nose-down motion of the airfoil section which decreases the angle of attack with increasing aerodynamic loads. This stabilizing effect was a key factor, added to other innovations, for the success of the Messerschmitt Me 262 jet fighter of WWII which later influenced the designs of post-war aircraft in the United States such as the F-86 Sabre and the Boeing B-47 Stratojet [14–16] among others. The second possible configuration is known as forward sweeping or structural divergence. Here, the aerodynamic coefficient reference point is forward to the wing torsional center causing the airfoil to increase the angle of attack in a nose-up motion as the aerodynamic loads increase. Experimental aircraft like the Grumman X-29 is based on this principle, where the aerodynamic instability of the wing configuration increased agility, but also required the use of advanced computerized control systems for piloting and composite materials on the blade structure to counteract the effects caused by the structural divergence [17,18], which can potentially lead to a complete structural collapse. In addition to adaptiveness effects, swept wings help delay the drag increment caused by fluid compressibility [19,20] at high Mach number regimes. Within the scope of this work, we will only focus on the structural-adaptiveness aspect of the swept-wing concept, which is the relevant one in terms of wind-turbine blade applications.

In this paper, we report some recent results we have obtained applying our code to the analysis of geometrical adaptive blades, taking full advantage of the coupled deformation modes that our aeroelastic code can represent. We will analyze alternative blade configurations for the NREL-5 MW wind-turbine [21], optimizing the design to mitigate vibration and improve fatigue performance.

2. Structural model: the dimensional-reduction technique for beams

Even though rotor blades and rotary wings are slender structures that may be studied as beams, they are usually not simple to model due to the inhomogeneous distribution of material properties and the complexity of their cross sections (see for example Fig. 2). The *ad hoc* kinematic assumptions made in classical theories (like the Bernoulli or the standard Timoshenko approaches) may introduce significant errors, especially when the beam is vibrating with a wavelength shorter than its length [22].

Proposed and developed by Prof. Hodges and his collaborators [7,8], the Dimensional Reduction technique is a model for curved

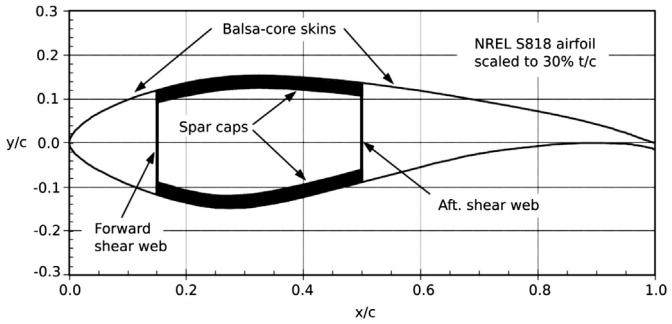

Fig. 2. An example of a wind-turbine blade internal structure representative of current commercial designs. The primary structural member is a box-spar, with a substantial build-up of spar cap material between the webs. The exterior skins and internal shear webs are both sandwich construction with triaxial fiberglass laminate separated by balsa core (from Ref. [23]).

and twisted composite beams that uses the same variables as classical Timoshenko beam theory, but the hypothesis of beam sections remaining planar after deformation is abandoned. Instead, the real warping of the deformed section is interpolated by a 2-D finite-element mesh and the strain energy is rewritten in terms of the classical 1-D Timoshenko's variables (see Fig. 3). The geometrical complexity of the blade section and/or its material inhomogeneousness is reduced into a stiffness matrix for the 1-D beam problem to be solved along the reference line that represents the axis of the beam. This reference line could be curvilinear (i.e. twisted or bent), which allows modeling of blades with initial curvature in their geometrical design. The reduced 1-D strain energy is equivalent to the actual 3-D strain energy in an asymptotic sense. Elimination of the *ad hoc* kinematic assumptions produces a fully populated 6×6 symmetric stiffness matrix for the 1-D beam, with as many as 21 coefficients, instead of the six fundamental stiffnesses of the original Timoshenko theory. That is why this technique is often referred to as a *generalized Timoshenko theory*. Even for the case of large displacements and rotations of the beam sections, dimensional-reduction allows for accurate modeling of the bending and transverse shear in two directions, extension and torsion of the structure as a 1-D finite-element problem. Thus, through dimensional-reduction we are able to decouple a general 3-D nonlinear anisotropic elasticity problem into a linear, 2-D, cross-sectional analysis (that may be solved *a priori*), and a

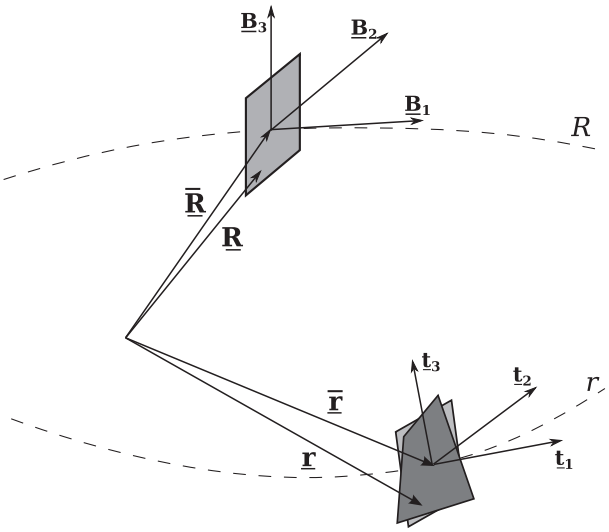

Fig. 3. Dimensional-reduction model: schematic of the reference line, orthogonal triads, and beam sections before and after deformation.

nonlinear, 1-D, beam ODE unsteady problem that is what we solve at each time step of the fluid–structure interaction analysis. The cross-sectional 2-D analysis (that may be performed in parallel for the many cross sections along the blade/wing) calculates the 3-D warping functions asymptotically and finds the constitutive model for the 1-D nonlinear beam analysis of the blade. After one obtains the global deformation from the 1-D beam analysis, the original 3-D fields (displacements, stresses, and strains) at each time step can be recovered *a posteriori* using the already-calculated 3-D warping functions.

Detailed descriptions of the development of both, the dimensional-reduction technique and the Variational Asymptotic Beam Section (VABS) model, can be found in Refs. [7,8], including validation tests for different cases of complex beams, and applications to helicopter and wind-turbine blades. A more comprehensive description of our implementation, followed by some results of the application of our code to the analysis of vibrational modes of composite laminate wind-turbine blades, is presented in Ref. [6].

3. Aerodynamic model: the large sectional rotation BEM (LSR-BEM)

The tendency in the wind-turbine industry to increase the size of the state-of-the-art machine [21] drives not only to bigger, but also to more flexible blades which are relatively lighter. It is observed for this type of wind turbine blades that big deformations, either due to blade flexibility or to pre-conforming processes, produce high rotations of the blade sections. Moreover, blades could be pre-conformed with specific curvatures given to any of their axes *(i.e. coning/sweeping)*. This tendency puts in evidence one of the most important limitations of the current BEM theory. While the basics of this theory keeps being perfectly valid, the actual mathematical formulation implies the assumption of blade sections remaining perpendicular to an outwards radial line contained in the plane of the actuator disk coincident with the rotor's plane. That is, even though the basics of the BEM theory (i.e. the equation of the aerodynamic loads and the change of momentum in the streamtubes) keeps being valid, the mathematical formulation cannot represent large rotations of the blade sections. This basically leads to a misrepresentation of the effects of the large deformation associated to flexible blades on the computation of the aerodynamic loads. Hence, a new mathematical formulation is required to project the velocities obtained from momentum theory onto the blade element's plane and then re-project backwards the resulting forces from Blade Element theory onto the plane of the stream tube actuator disk.

Here, we will introduce the new mathematical formulation of the BEM theory to take into account the large sectional rotations of blade elements out of the rotor's plane. We make use of linear operators that perform the rotation of the physical magnitudes involved (velocities, forces, etc.), consistent of a set of orthogonal matrices, see Ref. [24].

For instance, we could write the wind velocity vector W_h facing the differential annulus of our actuator disk, affecting its components, according to BEM theory, by the axial induction factor a and the rotational induction factor a':

$$W_h = \begin{bmatrix} W_{\mathrm{wh}_{(1)}}(1-a) \\ W_{\mathrm{wh}_{(2)}} + \Omega\, r_h(1+a') \\ W_{\mathrm{wh}_{(3)}} \end{bmatrix}, \tag{1}$$

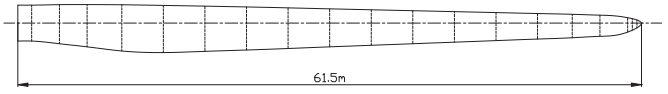

Fig. 4. Plan view of the blade indicating the position of the design blade sections.

where a and a' are the axial and tangential induction factors respectively, W_{wh} is the incoming wind velocity projected into the h coordinate system, Ω is the angular velocity of the rotor and r_h is the radial distance of the airfoil section in the h coordinate system. The h subscript here indicates that the wind velocity vector is described in the *hub* coordinate system according to standards from the International Electrotechnical Commission (IEC) [25].

Then, to compute the relative velocity affecting a blade element, we will project W_h going through the different coordinate systems, from the hub, until reaching the blade's section coordinate system. Let's see first which rotations we shall go through, and which matrices will transform our velocity vector from one coordinate system to the other.

Thus, the Pitching rotation matrix $\mathbf{C}_{\theta_p}$, represents a rotation around the pitch axis of the blade, which reflects any change in pitch introduced by the actuators of the control system:

$$\mathbf{C}_{\theta_p} = \begin{bmatrix} \cos(\theta_p) & -\sin(\theta_p) & 0 \\ \sin(\theta_p) & \cos(\theta_p) & 0 \\ 0 & 0 & 1 \end{bmatrix}, \tag{2}$$

where θ_p is the pitch angle. Similarly, the coning rotation matrix $\mathbf{C}_{\theta_{cn}}$, is a linear operator with a basic rotation taking into account the coning angle for the rotor. This could be a fixed angle representing the coning of the rotor as a constructive feature (as in the case of the NREL-5 MW reference wind turbine) or, if a control mechanism based on changing the coning angle is included, a variable matrix that reflects any control action in real time. For a detailed description of the concept of coning rotors and their effects see Refs. [26–28].

Two more reorientations are needed in order to get to the instantaneous system of coordinates of the blade sections, defined as r in previous sections (see Fig. 3). The first of these matrices contains information on blade section's geometry at the time the blade was designed and manufactured. As it was mentioned previously, the blade could have pre-conformed curvatures along its longitudinal axis *(i.e. the blade axis is no longer rectilinear)*. These curvatures can reflect either an initial twist along the longitudinal axis or a combination of twist plus pre-bending on the other two axes *(i.e. coning/sweeping)*. To this end, we compute during the blade design stage a set of transformation matrices which contain the information of the three dimensional orientation of the blade's sections for each position on the longitudinal axis as we move along the span. We compute the Frenet–Serret formulas that define the curvature of the (now curvilinear) longitudinal axis [29]. These differential formulas provide the means to describe the *tangent*, *normal* and *binormal* unit vectors on a given curve. Due to this unit vectors, the Frenet–Serret coordinate system is also known as the *TNB frame*. More information about the calculation of the TNB unit vectors, their properties and other applications can be found in Ref. [29]. Around the tangential axis of the TNB, there is a further rotation of each blade section to orient it accordingly to the particular twist specified on the blade's aerodynamic design.

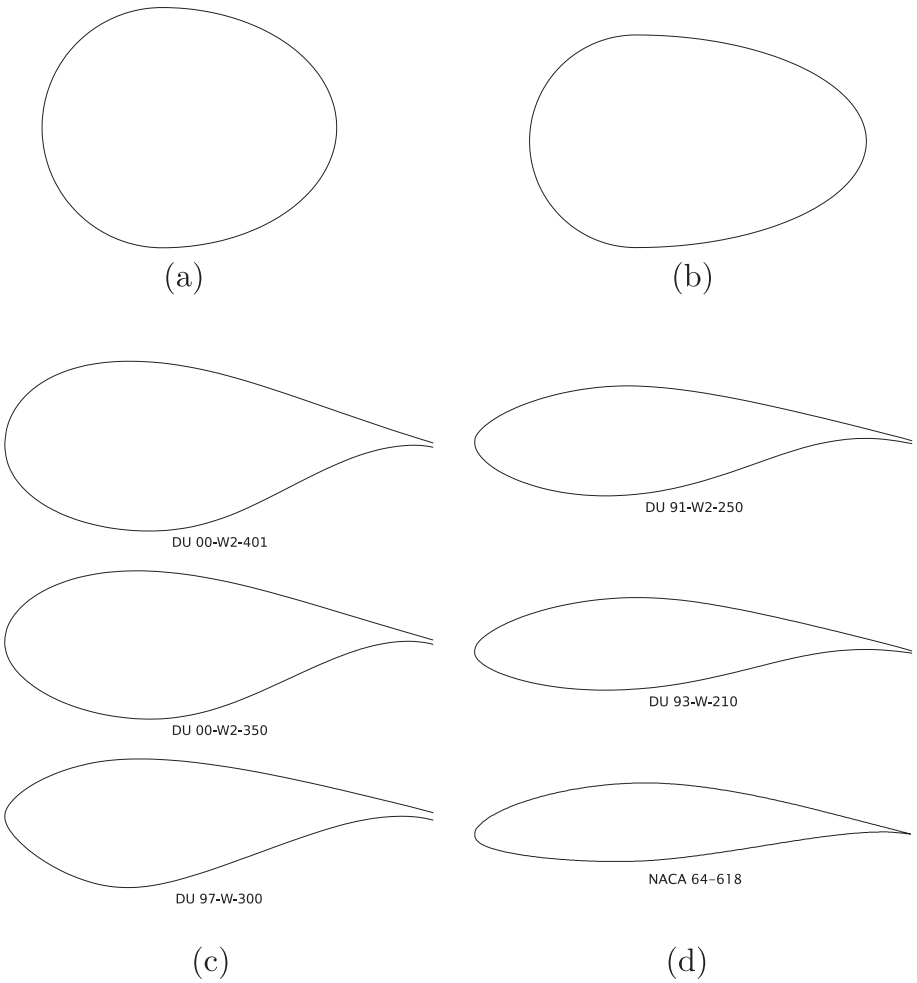

Fig. 5. Airfoil sections used to define the geometry of the blade: (a) and (b) ellipsoidal sections corresponding to stations 3 and 4, (c) thick airfoil shapes used in the inner regions, from station 5 to 8 of the blade-span, and (d) airfoil shapes used in the mid-span and tip regions of the blade-span.

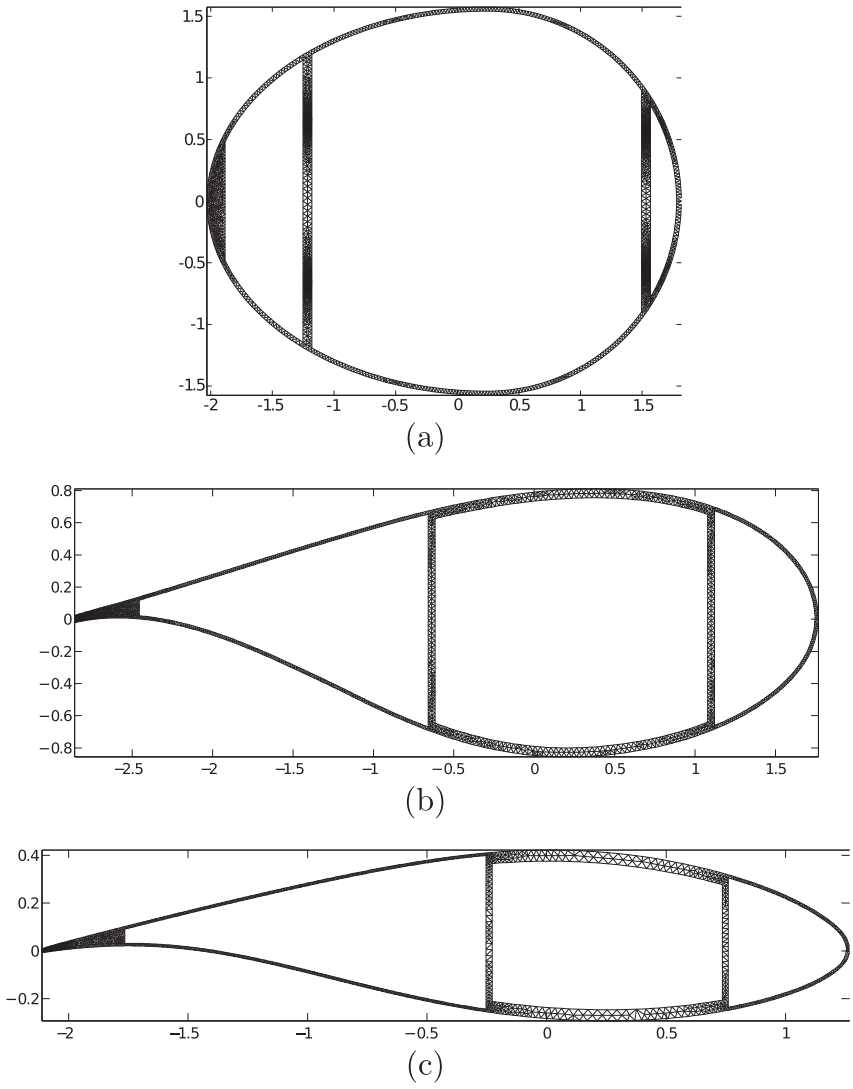

Fig. 6. Finite element meshes for: (a) transitional elliptical section, (b) morphed blade section located at the 20% of the blade span, and (c), morphed blade section located at the 60% of the blade span.

Combining these rotations we then create a transformation matrix for every blade section at different span positions. We call this matrix the $\mathbf{C_{Rb}}$, as it relates the global coordinate system of the blade b, with the system of coordinates of the blade sections in the undeformed configuration R (Fig. 3).

After applying the $\mathbf{C_{Rb}}$, one more projection is needed to get to the instantaneous coordinate system r (see Fig. 3). This last transformation is given by an orthogonal matrix $\mathbf{C_{rR}}$, computed by the 1D structural model. It contains information to transform vectors from the R to the r systems after structural deformations had occurred. Note that this matrix is updated at every time step of the 1D model during dynamic simulations, being one of the key variables transporting information between the structural and aerodynamic models.

Table 1
Operational parameters of the NREL-RWT.

Description	Value
Rating	5 MW
Rotor orientation	Upwind
Configuration	3 blades
Rotor, hub diameter	126 m, 3 m
Hub height	90 m
Rated wind speed	11.4 m/s
Rated rotor speed	12.1 rpm
Overhang	5 m
Rotor precone	2.5°

After all these projections of the W_h vector, we have the relative wind velocity expressed in the blade's section coordinate system, r. The expression for the flow velocity relative to the blade section, W_{rel}:

$$W_{\text{rel}} = \left(\mathbf{C_{rR}}\mathbf{C_{Rb}}\mathbf{C}_{\theta_p}\mathbf{C}_{\theta_{cn}}W_h\right) + v_{\text{str}} \tag{3}$$

where the addition of v_{str} corresponds to the blade section structural deformation velocities, coming from the structural model.

Then, the magnitude $|W_{\text{rel}}|$ and the angle of attack α are used to compute the forces on the airfoil section through the aerodynamic coefficients C_l, C_d. Another innovation of our model is that the data tables from static wind-tunnel are corrected at each time step to consider either rotational-augmentation, dynamic-stall effects, or both.

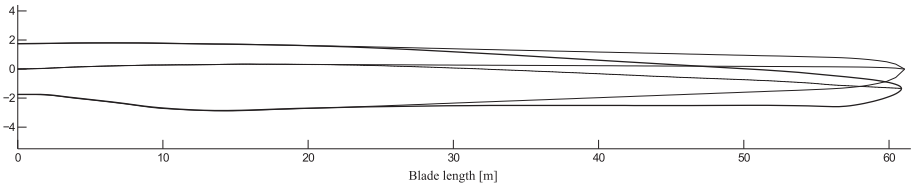

Fig. 7. Blade configuration comparison. Original (thin line) vs. swept-back (bold line) blade.

The aerodynamic loads acting on the blade element is then projected back onto the *h* coordinate system,

$$dF_h = \mathbf{C}^T_{\theta_{cn}}\mathbf{C}^T_{\theta_p}\mathbf{C}^T_{\mathbf{Rb}}\mathbf{C}^T_{\mathbf{rR}}\mathbf{C}_{\mathbf{Lthal}}dF_r \quad (4)$$

where $\mathbf{C_{Lthal}}$ is the matrix which projects the lift and drag forces onto the chord-wise and chord-normal directions, which are aligned with the coordinates of *r*. Finally, as in the classical BEM theory, $\mathbf{dF}_h$ is equated to the rate of change of momentum in the annular stream tube corresponding to the blade element. The component normal to the rotor's disk, is equated to the change in axial momentum, while the tangential component, is equated to the change of angular momentum.

In order to apply this theory to HAWT rotors, we must introduce some corrective factors into the calculation process. BEM theory does not account for the influence of vortices being shed from the blade tips into the wake on the induced velocity field. These tip vortices create multiple helical structures in the wake which play a major role in the induced velocity distribution at the rotor. To compensate for this deficiency in BEM theory, a tip-loss model originally developed by Prandtl is implemented as a correction factor to the induced velocity field [30]. In the same way, a hub-loss model serves to correct the induced velocity resulting from a vortex being shed near the hub of the rotor (see Refs. [3,31]) Another modification needed in the BEM theory is the one developed by Glauert [32] to correct the rotor thrust coefficient in the "turbulent-wake" state. This correction plays a key role when the turbine operates at high tip speed ratios, and the induction factor is greater than about 0.45.

BEM theory was originally conceived for axisymmetric flow. Often, however, wind turbines operate at yaw angles relative to the incoming wind, which produces a skewed wake behind the rotor. For this reason, the BEM model needs also to be corrected to account for this skewed wake effect [33,34]. The influence of the wind turbine tower on the blade aerodynamics must also be modeled. We implemented the models developed by Bak et al. [35] and Powles [36] which provide the influence of the tower on the local velocity field at all points around the tower. This model contemplates increases in wind speed around the sides of the tower and the cross-stream velocity component in the tower near flow field.

Our model also incorporates the possibility to add multiple data tables for the different airfoils, and use them in real-time according to the instantaneous aerodynamic situations on the rotor. It also uses the Viterna's extrapolation method [37] to ensure the data availability for a range of angles of attack $\pm 180^\circ$.

4. Numerical experimentation

In this section, we present a summary of the results of a series of numerical experiments on alternative geometrical-adaptive designs for rotor blades based on the *5-MW Reference Wind Turbine (RWT)* project developed by NREL [21]. Dynamic rotor responses under different operational conditions will be reported for the original blade geometry and two alternative configurations: one with forward, and the other with backward sweeping. A clear advantage of seeking blade adaptiveness by sweeping is that it mostly involves geometrical rearrangement of the blade sections along the axis of the mold where the blade is cast in while materials distribution as well as plying processes keep unchanged, making it an appealing option from the economic point of view.

Based on the REpower 5M wind turbine, the NREL's RWT was conceived for both onshore and offshore installations and it is well representative of state-of-the-art, utility-scale, multi-megawatt commercial wind turbines. Although full specific technical data is not available for the REpower 5M rotor blades, a baseline from a prototype blade was originally released by LM Glasfiber in 2001 for the *Dutch Offshore Wind Energy Converter (DOWEC) 6 MW* wind turbine project [38,39] and later readapted by NREL. This suite of reports is considered one of the most detailed sources of information available for large wind turbines to date. In addition, the NREL 5-MW RWT project has been adopted as a reference model by the integrated European Union UpWind research program [1] and the International Energy Agency (IEA) Wind Annex XXIII Subtask 2 Offshore Code Comparison Collaboration (OC3) [40–42].

4.1. Design of the original blade: aerodynamic properties and constructive aspects

As in NREL's RWT project [21], the length of our rotor blade is set to be 61.5 m. All basic aerodynamic properties as blade section chords, twist angles, and spanwise distribution of airfoil sections also correspond to the original data in Ref. [21]. Fig. 4 shows a plan view of the blade and the position of the 20 stations along the span where the design blade sections are located.

Stations 3 and 4 are transitional shapes providing a smoother transition from the cylindrical shape of the sections 1 and 2, to the first airfoil shape in station 5. Two ellipsoidal shapes were used which match the chords originally given in Ref. [21]. Fig. 5a and b shows the profiles of these two transitional shapes. Fig. 5c shows the profiles of the three thick airfoil sections corresponding to the inner regions of the blade, stations 5 to 8, where a good structural support is required, while Fig. 5d shows the three airfoils used in the remaining sections covering from the mid-span to the tip regions where aerodynamic efficiency is the priority. Aerodynamic coefficients for the airfoils were taken from Refs. [39,43]. Aerodynamic

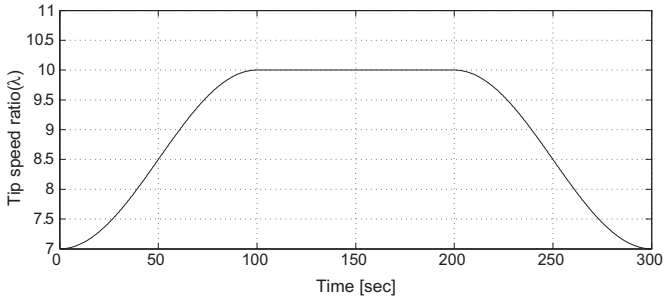

Fig. 8. Tip speed ratio evolution during blade adaptiveness simulations. Variation of the rotational speed of the turbine at constant rated wind speed (according to Table 1).

data for the cylinder, as well as the ellipsoidal shapes, were taken from Ref. [21].

Observing the internal structure of a blade section (see Fig. 2), we can see the aerodynamic shells plus two spar caps which, together with two shear webs, form the box-beam spar. Constructive characteristics as thickness as well as number and orientation of fiberglass layers for the different structural components of the blade sections are covered in detail in reports published by SANDIA National Labs [23,44]. According to these reports, the aerodynamic shells are mainly composed of $\pm 45^\circ$ layers, plus a small amount of randomly oriented fibers, gelcoat and filling resin. Shear webs, the box-beam lateral walls, are made up of $\pm 45^\circ$ layers with a balsa wood core which provides the needed buckling resistance. Shear webs are usually located at the 15% and 45% of the airfoil's chord but, for sections closer to the blade's root, the positions are modified in order to increase the section's stiffness. Focusing now on the spar caps, these are made of 0° layers and are the most important structural element as they give support to the bending loads on the blade. Finally, the blade sections have a reinforcement at its rear part, i.e. the trailing edge spline, also made up of 0° oriented fibers which supports the bending loads in the chord-wise direction. Reports [23,44] also provide a comprehensive description of lamination sequences and material properties.

A triquadrilateral mesh (see Ref. [45]) was generated for each one of these sections. Fig. 6 shows examples of triangulations for a transitional elliptical section, a section located at 20% of the blade-span (a thick airfoil from the inner region), and a section at 60% of the span (a thin airfoil from the mid-span region). Material properties were equivalent to those of the actual laminates as described above.

4.2. Simulation of the dynamic response under transient conditions

The general specifications of the turbine match the ones on NREL's report [21], which are summarized in Table 1. Thus, the rotor has an upwind orientation, and it is composed of three 61.5 m long blades.

Based on the standard blade-sections distribution shown in Refs. [21], we first propose an alternative configuration modifying the position of the blade's longitudinal axis (i.e. the reference line of the equivalent beam) starting at 60% of the span, from the original value of 0.375 of the chord length from the airfoil's leading edge,

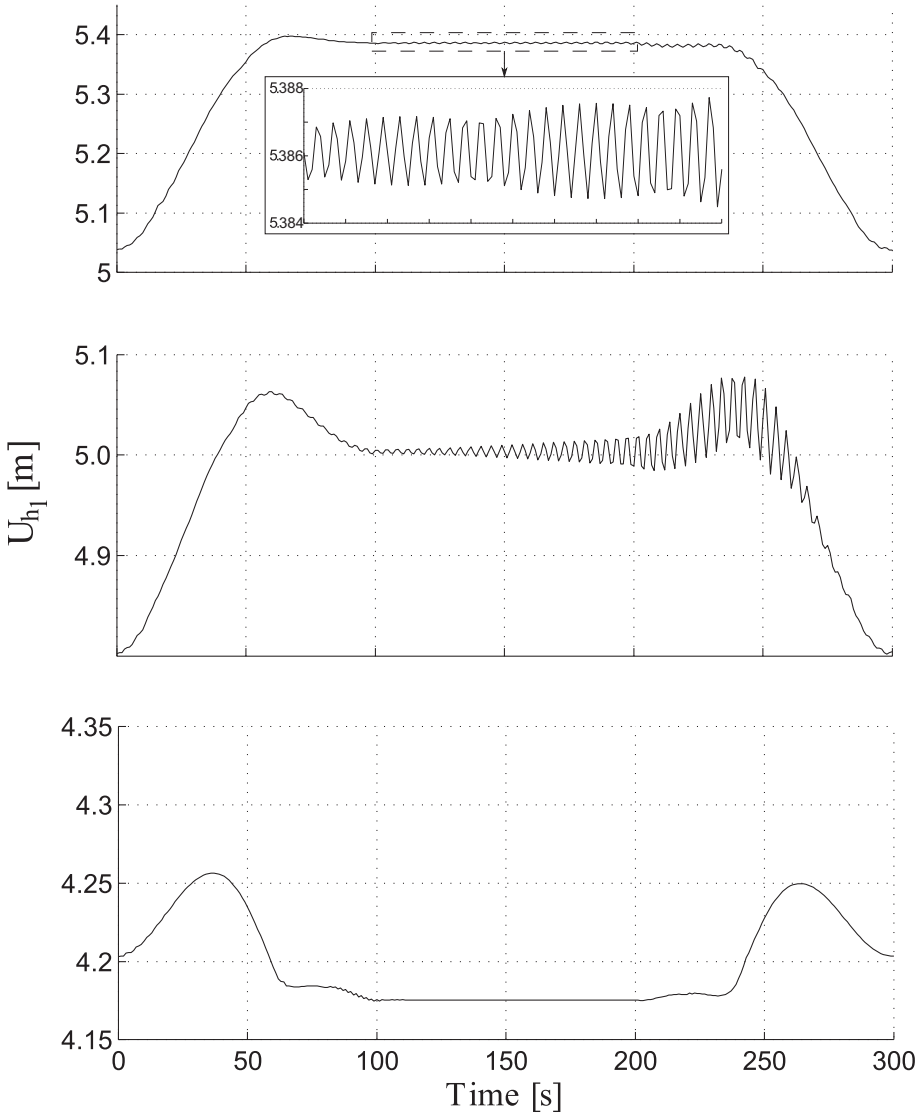

Fig. 9. Time evolution of the displacement perpendicular to the rotor disk for a section located at 95% of the blade span, according to Fig. 8. From top to bottom, original blade, forward-swept blade, and backward-swept blade.

increasing linearly up to 0.410 at 100%. This first configuration results in a slightly forward swept blade shape. The second alternative configuration is a more extended modification of this parameter, which now starts at 30% of the blade span, and gradually decreases from its original value towards the blade tip. In this latter case, the intention was to obtain the same structural behavior as in a swept-back blade, with a minimum modification of the manufacturing process. Fig. 7 shows a superposition of the plan shape of the second alternative blade over the original blade.

In order to test the aeroelastic dynamics of these blade configurations under transient conditions, we designed simulation where the rotor is accelerated beyond the rated operational speed, and then returned back to its nominal regime. We start from the nominal tip speed ratio of λ=7, and let the rotor speed up to λ=10 varying only the rotational speed of the turbine. The rotor then stays in this regime for a certain period of time, where we can observe its vibrational dynamics, and afterwards it reduces its rotational speed coming back down to λ=7. This evolution could be representative of a generic transient situation in which the rotational regime of the rotor is varied as the result of the action of the control system or the mechanical response of the drive train. More specific situations involving particular control strategies would be analyzed in the future. Fig. 8 shows the time evolution of the tip speed ratio during the 300 s of the simulation period. The acceleration and deceleration ramps have a sinusoidal shape.

Fig. 9 shows the time evolution of the displacement of the blade in the direction perpendicular to the rotor disk U_{h_1}, at a point located at 95% of the blade span, for the three blade configurations. Figs. 10 and 11 show respectively the thrust and torque exerted on the main shaft, and Fig. 12 shows the power output. In all these plots, we could identify a common pattern of behavior for each one of the blade configurations, which is clearly consistent with the theoretical principles of the swept blades mentioned above. In the case of the original blade, the location of the blade axis at 0.375 of the chord length puts the aerodynamic center 0.125 of a chord length ahead of the blade axis. For the type of airfoil used in this blade, and the flow's angle of attack when the turbine operates close to nominal conditions, this puts the blade axis approximately at the center of pressure (i.e. the point of application of the aerodynamic force). If the blade axis had been located at the aerodynamic center, there would have been an aerodynamic pitch moment acting in the nose-down sense producing a twist that would have reduced the angle of attack. In other words, the original design includes a forward sweep specifically intended to minimize the torsional deformation (and hence, the change in the angle of attack) when the blade operates around the nominal regime. This also puts the blade at the limit of aeroelastic stability, which is the reason why the oscillations appearing at the moment of deceleration when the regime is stabilized at λ=10 are neither amplified nor mitigated but remain at roughly the same level.

For the case of the first alternative blade, where the forward sweep was increased, the aeroelastic stability is further reduced to the point that, even with a slight sweep forward from the original design, the oscillations are amplified. This affects not only geometrical quantities like the flap-wise deformation (see Fig. 9), but also the torque, the thrust, and the power output. If the forward sweep is further increased, we will soon reach a point where the oscillations become so large that they will induce structural failure. On the other hand, the backward-swept blade, as it was expected, has the tendency of minimizing the oscillations, as could be seen in all the plots. We made a series of tests with different configurations of backward sweep, and selected the second option described above as a very interesting example on how mitigation of those

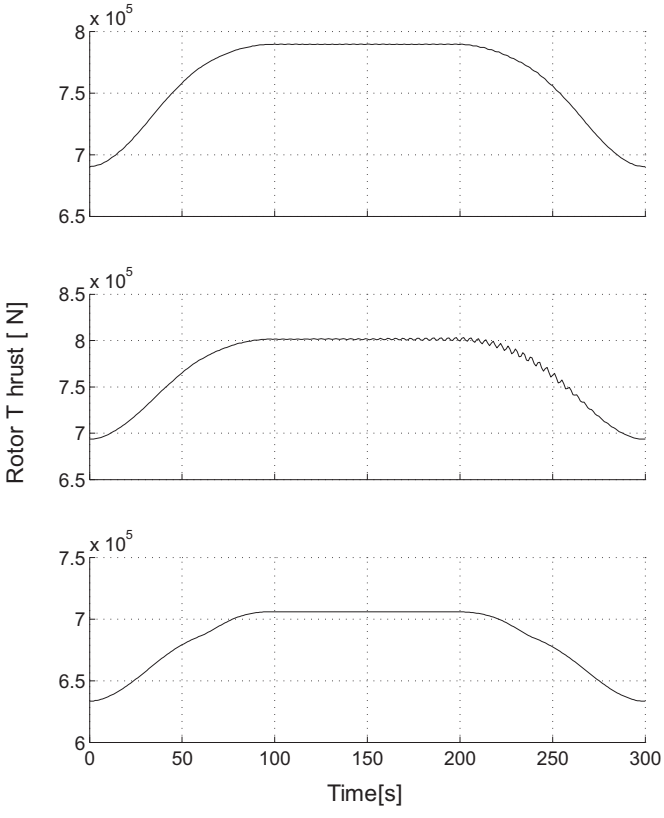

Fig. 10. Time evolution of the rotor thrust force, according to Fig. 8. From top to bottom, original blade, forward-swept blade, and backward-swept blade.

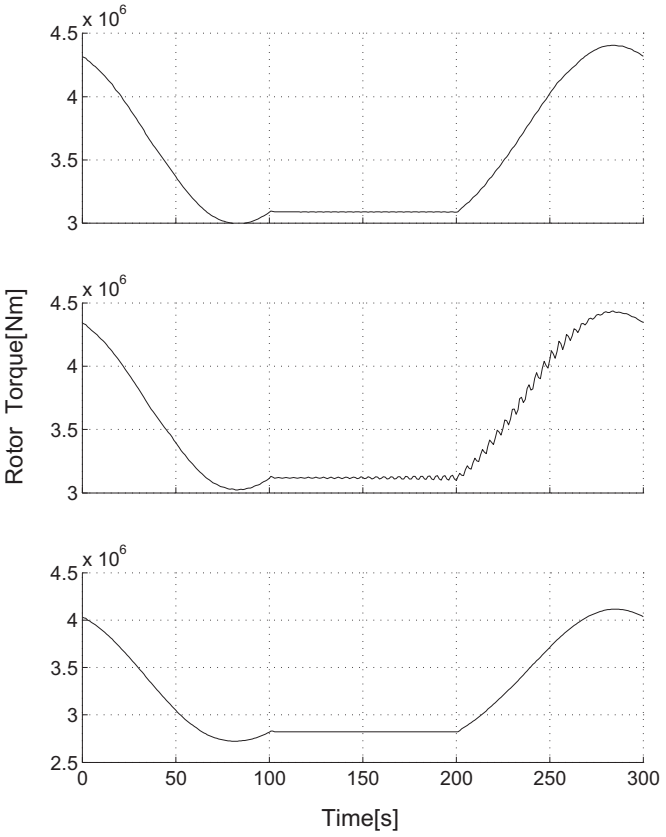

Fig. 11. Time evolution of the rotor torque, according to Fig. 8. From top to bottom, original blade, forward-swept blade, and backward-swept blade.

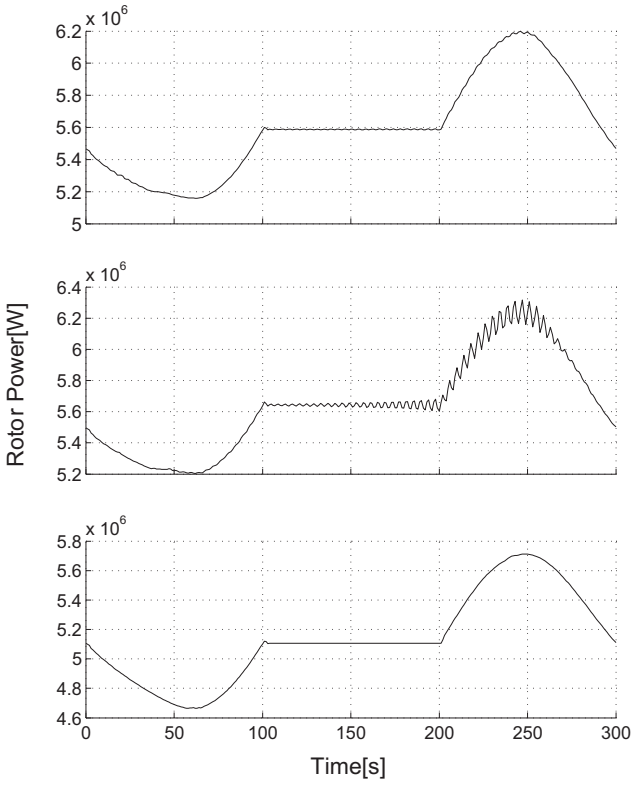

Fig. 12. Time evolution of the rotor's output power, according to Fig. 8. From top to bottom, original blade, forward-swept blade, and backward-swept blade.

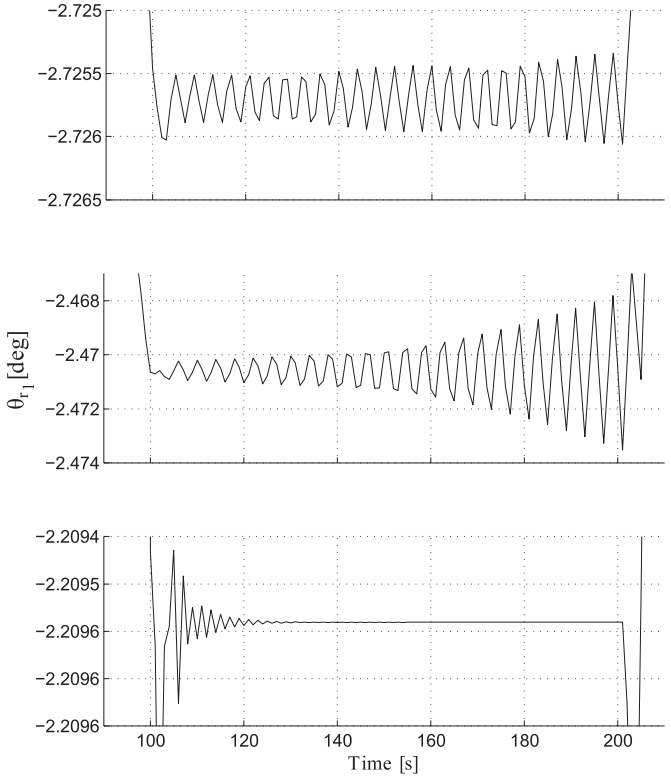

Fig. 13. Time evolution of the blade section torsion angle for a section located at the 95% of the blade span, according to Fig. 8, and referred to the *r* coordinate system according to Fig. 3. From top to bottom, original blade, forward-swept blade, and backward-swept blade.

fluctuations could be achieved by this relatively simple process of redesign. Some further discussion about how those fluctuations may affect several aspects of the operational life of the turbine will be presented in the concluding section. Note that the plots of the magnitudes depicted in Figs. 9–12 for the original blade begin from and continue at different value levels than the other two graphs in each figure. This is due to the fact that the twist angle at a certain operational condition is different for the swept-back and swept-forward blades (see Fig. 13), and it indicates that sweeping has effects on the mean values of the magnitudes as well as their fluctuations. These differences would be naturally compensated by the pitch control system by adopting a set point which would be different from the one of the original blade for the same operational conditions.

Finally, Fig. 13 shows the time evolution of the blade torsional deformation θ_{r_1}, which directly affects the angle of attack (and hence, the aerodynamic loads on the blade section) initiating the chain of events that ultimately leads to the evolution of the other variables. Here, we can clearly see how the amplitude of the oscillations in the torsion angle remain mostly constant in the original blade, but are amplified in the forward-swept blade, and quickly damped in the backward-swept blade. In a sense, the coupling of the aeroelastic combination could act either as a damper or an amplifier, depending on how the blade is designed. In the case of a damper, it would behave in the same sense as a viscous dissipation in the material. This could be related to the eigenvalues of the aeroelastic response of the blade/fluid as a system, the imaginary part of the eigenvalues would give the frequencies of the vibrational modes, while their real parts would reflect the effect either of the damping or the amplification of the aeroelastic coupling.

This analysis also confirms the important role played by the flexo-torsional modes of deformation that our model can take into account. This requires that both the structural and the flow modules could reflect the effects of the combined modes of deformation on the aerodynamic loads exerted on the blade sections. It is worth to mention that these features are absent in previous aeroelastic models like the FAST-Aerodyn suite [46–48].

5. Conclusions and outlook for further work

We have successfully developed a very powerful computational tool for the aeroelastic analysis of wind-turbine blades. Due to the particular features mentioned above in terms of a full representation of the combined modes of deformation of the blade as a complex structural part and their effects on the aerodynamic loads, it constitutes a substantial advancement ahead the state-of-the-art aeroelastic models currently available, like the FAST-Aerodyn suite [46–48]. Both the structural and the aerodynamic modules could reflect the effects of the combined modes of deformation on the aerodynamic loads exerted on the blade sections, features which are absent in previous aeroelastic models.

Here, we also include the results of several experiments on the NREL-5 MW blade, which is widely accepted today as a benchmark blade, together with some modifications on its geometrical design intended to explore the capacities of the new code in terms of capturing features on blade-dynamic behavior which are normally overlooked by the existing aeroelastic models. In this regard, some further remarks could be added to the observations already made about those experiments in Section 4.2:

First, the analysis presented here clearly confirms the important role played by the flexo-torsional modes of deformation, that our model can take into account, in the determination of the characteristics of the blade in terms of adaptiveness.

Second, even tough fluctuations in the aerodynamic loads may not necessarily lead to catastrophic failure (unless a very high level of structural divergence is inherent to the design), their mitigation is critical to avoid structural fatigue, which is a determining factor in blade lifespan. There are also many other components on the wind turbine that are directly affected by the level of fluctuation in the aerodynamic loads on the blades. For instance, the thrust and torque on the main shaft (see Figs. 10 and 11) directly affect the design of several wind-turbine components like the gearbox, couplings, bearings and the rotor's main shaft [3,31]. Moreover, the fluctuations in the torque are also reflected as fluctuations in power output (see Fig. 12), this may affect several other subsystems of the turbine like the generator, the power electronics, and other electrical systems involved, with effects which, if strong enough, may even propagate to the electric grid.

Third, as an outlook for further work, in view of the results presented here, we may explore the possibility of modifying the orientation of the fibers in the composite laminates used in blade construction. Together with other modifications in the layout of the internal structure of the blade, it could be expanded and complemented by suitable geometrical modifications of the aerodynamic design in such a way of increasing the effects of vibrational mitigation reported here. It could also be possible to achieve some degree of power limitation at high wind speeds, which in combination with flaps, micro-tabs, or other small flow-control devices, would reduce the size (or completely eliminate) the need of expensive pitch-control actuators. To this end, further experiments with swept-back blades with fully curvilinear axis seem to be particularly promising.

Acknowledgments

The authors are very grateful for the financial support made available by the National Science Foundation through grants CEBET-0933058 and CEBET-0952218, University of Buenos Aires through grant 20020100100536 UBACyT 2011/14.

References

[1] UpWind project. http://www.upwind.eu/; 2010 [accessed May 2012].
[2] NREL. Wind power today. Report DOE/GO-102005–2115. U.S. Department of Energy; 2005.
[3] Manwell JF, McGowan JG, Rogers AL. Wind energy explained: theory, design and application. Chichester, UK: Wiley; 2002.
[4] Griffin D. Windpact turbine design scaling studies technical area 1œcomposite blades for 80-to 120-meter rotor. Tech. Rep. SR-500–29492. NREL; 2001.
[5] Hansen MOL, Sørensen JN, Vousitas S, Sørensen N, Madsen HA. State of the art in wind turbine aerodynamics and aeroelasticity. Prog Aerosp Sci 2006;42:285–330.
[6] Otero AD, Ponta FL. Structural analysis of wind-turbine blades by a generalized Timoshenko beam model. J Solar Energ Eng 2010;132(1):011015–8.
[7] Yu W, Hodges DH, Volovoi V, Cesnik CES. On Timoshenko-like modeling of initially curved and twisted composite beams. Int J Sol Struct 2002;39:5101–21.
[8] Hodges DH. Nonlinear composite beam theory. Reston, Virginia: AIAA; 2006.
[9] Griffin DA. Evaluation of design concepts for adaptive wind turbine blades. Report SAND2002–2424. Sandia National Laboratories; 2002.
[10] Locke J, Contreras Hidalgo I. The implementation of braided composite materials in the design of a bend-twist coupled blade. Report SAND2002–2425. Sandia National Laboratories; 2002.
[11] NREL, 20% wind energy by 2030: increasing wind energy's contribution to U.S. electricity supply. Report DOE/GO-102008–2567. U.S. Department of Energy; 2008.
[12] Meirer HU. German development of the swept wing 1935–1945 (originally published in german as die deutsche luftahrt die pfeilflügelentwicklung in deutschland bis 1945, bernard & graefe verlag, 2006). AIAA Library of Flight; 2010.
[13] Anderson JD. A history of aerodynamics. McGraw Hill; 1997.
[14] O'Connell D. Messerschmitt Me 262: the production log 1941–1945. Leicestershire, UK: Classic Publications, ISBN 1-903223-59-8; 2006.
[15] Foreman J, Harvey S. The Messerschmitt Me 262 Combat Diary. Surrey, UK: Air Research Publications, ISBN 1-871187-30-3; 1990.
[16] Blair M. Evolution of the F-86. In: AIAA Evolution of Aircraft Wing Design Symposium. 1980.
[17] Thruelsen R. The Grumman story. New York: Praeger Publishers, Inc, ISBN 0-275-54260-2; 1976.
[18] Winchester J. Grumman X-29. X-Planes and prototypes. London: Amber Books Ltd, ISBN 1-904687-40-7; 2005.
[19] Barmby JG, Cunningham HJ, Garrick IE. Study of effects of sweep on the flutter of cantilever wings. National Advisory Committee for Aeronautics; 1951.
[20] Hilton WF, L.B., Berk G. High-speed aerodynamics. Longmans, Green and Co; 1952.
[21] Jonkman J, Butterfield S, Musial W, Scott G. Definition of a 5-MW reference wind turbine for offshore system development. Tech. Rep. NREL/TP-500–38060. National Renewable Energy Laboratory; 2009.
[22] Yu W, Hodges DH. Generalized Timoshenko theory of the variational asymptotic beam sectional analysis. J Am Helicopter Soc 2005;50:46–55.
[23] Griffin DA. Blade system design studies volume I: composite technologies for large wind turbine blades. Report SAND2002–1879. Sandia National Laboratories; 2002.
[24] Goldstein H. Classical mechanics. 2 ed. Addison-Wesley; 1980.
[25] IEC. Wind turbine generator systems – part 13: measurement of mechanical loads. Report IEC/TS 61400–13. International Electrotechnical Commission (IEC); 2001.
[26] Jamieson P. Innovation in wind turbine design. Wiley; 2011.
[27] Crawford C. Re-examining the precepts of the blade element momentum theory for coning rotors. Wind Energ 2006;9(5):457–78.
[28] Crawford C, Platts J. Updating and optimization of a coning rotor concept. J Solar Energ Eng 2008;130:031002.
[29] Yamaguchi F. Curves and surfaces in computer aided geometric design. Berlin: Springer-Verlag; 1988.
[30] Glauert H. Airplane propellers. Aerodyn Theory 1935;4:169–360.
[31] Burton T, Sharpe D, Jenkins N, Bossanyi E. Wind energy handbook. Chichester, UK: Wiley; 2001.
[32] Glauert H. A general theory of the autogyro. British ARC; 19261111.
[33] Pitt DM, Peters DA. Theoretical prediction of dynamic-inflow derivatives. Vertica 1981;5(1):21–34.
[34] Leishman JG. Principles of helicopter aerodynamics. Cambridge, UK: Cambridge University Press; 2006.
[35] Bak C, Aagaard Madsen H, Johansen J. Influence from blade-tower interaction on fatigue loads and dynamic (poster). In: Wind energy for the new millennium. Proceedings. 2001 European wind energy conference and exhibition (EWEC'01). 2001, p. 2–6.
[36] Powles SRJ. The effects of tower shadow on the dynamics of a horizontal-axis wind turbine. Wind Eng 1983;7:26–42.
[37] Viterna LA, Janetzke DC. Theoretical and experimental power from large horizontal-axis wind turbines. Tech. Rep.; National Aeronautics and Space Administration. Cleveland, OH (USA): Lewis Research Center; 1982.
[38] Kooijman HJT, Lindenburg C, Winkelaar D, van der Hooft EL. Dowec 6 MW pre-design. Tech. Rep.; ECN-CX-01–135. Petten: Energy Research Center of the Netherlands; 2003.
[39] Lindenburg C. Aeroelastic modelling of the LMH64-5 blade. Petten: ECN; December 2002.
[40] IEAWIND. IEA wind, subtask 2: research for deeper waters. http://www.ieawind.org/AnnexXXIII/Subtask2.html; 2010 [accessed December 2011].
[41] Jonkman J, Butterfield S, Passon P, Larsen T, Camp T, Nichols J, et al. Offshore code comparison collaboration within IEA Wind Annex XXIII: Phase II results regarding monopile foundation modeling. In: 2007 European Offshore Wind Conference & Exhibition, 4–6 December 2007, Berlin, Germany. 2007.
[42] Passon P, Kühn M, Butterfield S, Jonkman J, Camp T, Larsen T. OC3–Benchmark exercise of aero-elastic offshore wind turbine codes. J Phys: Conf Ser 2007;75:012071. IOP Publishing.
[43] Timmer WA. comunicación personal; 2007.
[44] TPI Composites Inc. Parametric study for large wind turbine blades. Report SAND2002–2519. Sandia National Laboratories; 2002.
[45] Ponta FL. The KLE method: a velocity-vorticity formulation for the Navier-Stokes equations. J Appl Mech 2006;73:1031–8.
[46] Jonkman JM, Buhl Jr ML. Fast user's guide. Tech. Rep. NREL/EL-500–38230. Golden, Colorado, USA: National Renewable Energy Laboratory (NREL). http://wind. nrel. gov/designcodes/simulators/fast; 2005.
[47] Moriarty P, Hansen A. (US), N.R.E.L., Engineering, W. Aerodyn theory manual. National Renewable Energy Laboratory; 2005.
[48] Laino D, Hansen A. User's guide to the wind turbine aerodynamics computer software aerodyn. Tech. Rep. National Renewable Energy Laboratory under subcontract No. TCX-9-29209-01; 2002.